Optics and Lasers in Engineering 150 (2022) 106835

Contents lists available at ScienceDirect

Optics and Lasers in Engineering

journal homepage: www.elsevier.com/locate/optlaseng

Optical control for solar mirrors

D. Fontani, P. Sansoni*, F. Francini, D. Jafrancesco

CNR-INO National Institute of Optics, L.go Enrico Fermi 6, Firenze 50125, Italy

ARTICLE INFO

Keywords:
Optical control
Solar mirror
Profilometry

ABSTRACT

Concentrated power on the receiver and homogeneity of irradiance distribution are optimised in the optical design of solar mirrors. However, the manufactured mirror may contain some fabrication defects, which alter the irradiance distribution on the receiver. Surface defects introduce aberrations that cause an enlarged spot on the receiver and the resulting energetic losses depend on the collection features of each solar plant. To minimise these losses, it is essential to control the surface curvature, especially on large solar reflectors like heliostats. Facility of application, low-cost equipment, and elaboration simplicity are the key advantages of the proposed optical control. Exploiting techniques of image analysis, it assesses the mirror surface quality comparing an acquired image with a reference image. The application requires only a photographic camera and a screen with a calibrated pattern. The surface defects of the reflecting surface appear as deformations in the image of the pattern. This optical measurement could be adapted to examine mirrors with various shapes and sizes. It is an optical control that can be applied during manufacturing of the mirrors or on the produced samples.

1. Introduction

The installation of a heliostat field for a solar tower plant is a complex operation that requires the knowledge of the characteristics of all the single heliostats composing the field. Due to efficiency constrains, the dimension of the luminous spot of the receiver must be as small as possible. Considering this spot minimization, it is necessary to know the curvature of each single mirror, which is related to the focal length of the mirror, because an incorrect curvature of the heliostat can influence the shape of the luminous spot on the target.

Systems that allow to investigate the profile of the mirrors, thus to calculate the focal length or the curvature of the mirrors, are available. However, these methods of investigation are in general slow, and they require the preparation of complex equipment, especially if the samples to be examined are very numerous. This is precisely the case of a heliostat field, where hundreds of solar mirrors are arranged to concentrate the sun's rays in a receiver located on top of a tower.

In general, optical controls applied to detect surface profile defects are based on techniques of geometrical optics [1]. This section shows a brief review on the most common techniques used in the state of the art: Photogrammetry, Laser scanning profilometry, Tube reflection with a distant observer, Structured light on opaque covering, Deflectometry.

Photogrammetry [2,3] is a widespread technique for the numerical reconstruction of a three-dimensional object. It involves the use of a series of photographs of targeted objects, taken from a range of different perspectives. This is a very long activity that can take up to a day for a single module, and the resolution directly depends on the number of targets used. Stynes et al. [4,5] describe a method employing a high-performance radio-controlled helicopter, holding a specialised camera, which is a part of a photogrammetric data acquisition system. The device identifies reflector slope errors and misalignment of the receiver absorber with respect to the focal line of the parabolic trough collector. King et al. in [6] discuss the development and validation of a portable photogrammetry technique, which has been used to measure the shape of large mirror facets for solar collectors.

Laser scanning profilometry [7,8] is a well consolidated technique for surface control on mirrors. It is able to analyse a specular surface by studying the reflection of a laser beam projected on it.

The method of tube reflection with a distant observer [9–12] is specifically addressed to examine Parabolic Trough Collectors (PTCs). PTCs are composed of a linear parabolic mirror that focuses the sunlight on a tubular absorber, where a suitable fluid flows. The surface check technique exploits the geometry of the solar concentration system. A distant observer watching the concentrator observes the reflected image of the absorber tube, magnified due to the concentrating optics. The deformations of the image reflected by the parabolic mirror can indicate local defects on the collector or even a global distortion affecting the mirror. If a reference grid is superimposed to the tube, the resolution of the detection improves.

Structured light projection (SLP) consists in designing a pattern with well-known characteristics, which will be projected on the object under inspection. In particular, the pattern is studied to evidence specific features of the object. The application of SLP techniques on reflective

* Corresponding author.
E-mail address: paola.sansoni@ino.cnr.it (P. Sansoni).

https://doi.org/10.1016/j.optlaseng.2021.106835
Received 12 January 2021; Received in revised form 13 July 2021; Accepted 1 October 2021
Available online 9 October 2021

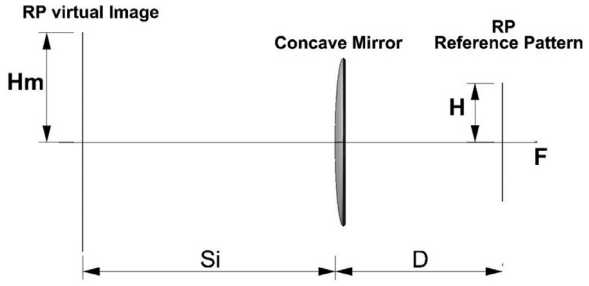

Fig. 1. Image created by a concave mirror.

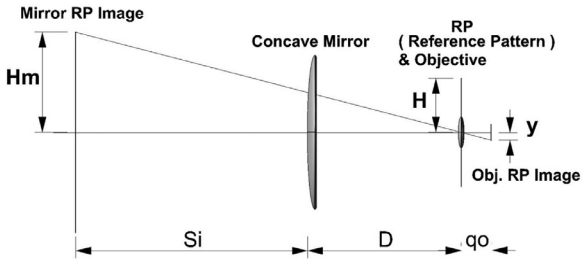

Fig. 2. Image captured by a camera.

or non-reflective surfaces has different measurement set-ups and elaboration procedures. A SLP technique for non-reflective surfaces can be applied to inspect an opaque covering of the mirror [13–15]. This technique uses a Moiré pattern projected onto an opaque layer that covers the mirror under inspection. The protective cover is only removed after the mirrors have been permanently mounted on the support structure.

Deflectometry [16–22] techniques are the application of the principles of SLP to a reflecting object, instead of observing an opaque object. In these techniques, the deformed pattern is not observed on the object but on a screen after having been reflected by the mirror under test. Deflectometry can be used to deduce surface slopes. Any irregularities in the object give rise to a distortion of the observed pattern, which can be evaluated quantitatively. The review of phase measuring deflectometry by Huang et al. [16] evidences how modern deflectometry has evolved in recent years. In [17] a null phase measuring deflectometry is presented to measure the three-dimensional shape of aspheric mirrors with radial symmetry. Han at al. [18] describe the use of a precise square planar mirror for the calibration of a phase measuring deflectometry system.

The proposed technique assesses the mirror curvature examining the image reflected by the heliostat. It does not require the employment of a projector, but only a Reference Pattern, a photographic camera, and a screen with heliostat sizes. The surface defects of the mirror appear as deformations in the photographic image of the pattern. With a simple processing, it is possible to obtain the data of the local curvature of the examined heliostat. For industrial controlling the reference image can be taken once for all and the camera can be placed at a fixed distance from the tested mirrors. The main advantages are facility of application, low-cost equipment, and elaboration simplicity.

2. Method to obtain the curvature radius Rc of a spherical surface

An ideal heliostat produces an enlarged virtual image if a reference object is placed between the focus and the mirror (Fig. 1). For a concave mirror with a long focal length, the Reference Pattern and the camera should be placed between the focus and the mirror.

Fig. 1 shows a concave mirror that forms a virtual image of height H_m of a Reference Pattern RP of height H. The virtual image is seen enlarged if the position of the object (RP) is between the mirror and its focus F.

For the concave mirror, in the conditions shown in Fig. 1, the magnification factor is

$$M = S_i/D = H_m/H \tag{1}$$

Where S_i is the distance between the virtual image and the mirror and D is the distance between the mirror and the Reference Pattern.

Moreover, considering the relationship with the radius of curvature Rc

$$1/D - 1/S_i = 2/Rc \tag{2}$$

it is possible to obtain the curvature Rc of the concave mirror by the following expression:

$$Rc = 2/\left(\frac{1}{D} - \frac{1}{S_i}\right) \tag{3}$$

From the radius of curvature Rc it is possible to obtain the focal length as: $f = Rc/2$.

However, S_i and H_m are values that cannot be measured directly, so a method was developed to find the S_i value using a camera.

The method for acquiring the image with a camera is outlined in Fig. 2. The camera is in the same plane as RP and acquires, on its focal plane, the image reflected by the mirror, which is a real image of height y. In Fig. 2, for simplicity, the camera lens is represented by a simple lens, whose position coincides with that of RP.

The image of the Reference Pattern produced by the concave mirror is recorded with a reduction factor k, expressed by

$$k = q_o/(S_i + D) \tag{4}$$

where q_o is the distance between the image plane of the camera and the camera lens.

Then

$$y = k \cdot H_m \tag{5}$$

y is obtained from the acquired image by counting the number of pixels N_i[1] and knowing the size Δ of the pixel in microns. Therefore

$$y = N_i \cdot \Delta = k \cdot H_m \tag{6}$$

and it is obtained

$$H_m = N_i \cdot \Delta \cdot (S_i + D)/q_o \tag{7}$$

H_m is the size of the virtual image produced by the mirror and measured with the camera. If q_o and Δ are known precisely it is possible to obtain the value of S_i by the following expression:

$$S_i = (y \cdot D^2)/(q_o \cdot H - y \cdot D) \tag{8}$$

Once the image-mirror distance S_i is known it is possible to obtain the radius of curvature Rc from Eq. (3).

Nevertheless, it is not always possible to know q_o precisely because its value depends on various factors; the main two are: focusing operation of the camera and complexity of the camera objective. Moreover, the value of Δ must be carefully obtained because it affects the resolution of the encoding with which the acquired image was recorded.

Since it is difficult to obtain the real values of q_o and Δ, the proposed technique tries to avoid the assessment of these two parameters. This technique involves recording a reference image, as shown in Fig. 3. This reference image is taken after having removed the concave mirror and placing the Reference Pattern at a 2D distance from the lens, without modifying the position and settings of the camera. The choice of the 2D

[1] The explanation refers to the vertical axis, but it can also be applied to the direction perpendicular to the plane of Fig. 2. This depends on the characteristics of the camera utilized.

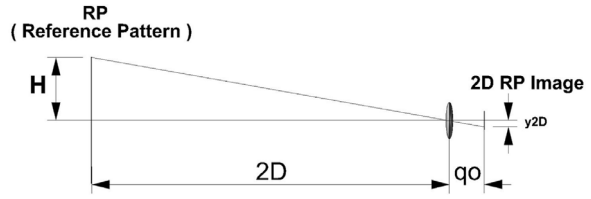

Fig. 3. Configuration for taking the Reference Pattern image.

distance is justified by the fact that it is equivalent to take the reference image with a flat mirror placed at a distance *D*.

With the configuration of Fig. 3 the *H* dimension of the Reference Pattern and its image size y_{2D} on the camera (plane) are linked by the following equation:

$$H = y_{2D} \cdot 2D/q_o = N_{2D} \cdot \Delta \cdot 2D/q_o \tag{9}$$

where N_{2D}[2] is the number of pixels in this case.

Considering the ratio

$$K_p = N_i/N_{2D} \tag{10}$$

between the pixels number N_i for the configuration in Fig. 2 and the pixels number N_{2D} for the configuration in Fig. 3, it is possible to obtain the new expression of the image-mirror distance S_i:

$$S_i = (K_p \cdot D)/(2 - K_p) \tag{11}$$

3. Validation

In order to validate the described procedure for obtaining the curvature radius Rc some measurements were performed on a concave mirror with a known focal length. Two types of tests were carried out: the first one consists in the determination of Rc on a known concave mirror; while the second one consists in the exam of the surface of a plane mirror.

For the first exemplificative test, the characteristics of the sample mirror were 6 inches of diameter (152.4 mm) and 60 inches of focal length (1524 mm), which corresponds to a curvature radius of 120 inches (3048 mm). This mirror was chosen because it is a calibrated mirror, and the known focal length is ten times the diameter. The f-number f# is 10 (the focal length divided by the diameter); it is small compared to those of the heliostats (typically for a small solar field f# is greater than 12), but not so far from their f#. However, it is sufficient to validate the methodology allowing to perform the measurement in laboratory.

For having a length reference, a simple ruler was selected as Reference Pattern. Fig. 4 shows the photo of the virtual image of the ruler, taken through the concave mirror. The measurement layout to capture the picture of Fig. 4 is the scheme shown Fig. 3.

Various measurements were performed with different distances (*D*) between the mirror and the Reference Pattern, always keeping the Reference Pattern between the mirror and the focal point. To take the photos of the virtual images, the camera and the ruler were always placed on the same plane, and they were shifted with respect to the sample mirror. To take the corresponding reference images with the layout of Fig. 3, the ruler was placed at a 2D distance from the camera.

The procedure described in Section 2 was applied to the acquired images. The results obtained are shown in Table 1, for three RP-mirror distances. The table reports: distance between concave mirror and Reference Pattern (D), height of the Reference Pattern (H), ratio between the pixel numbers (K_p), distance of the virtual image from the mirror (S_i), radius of curvature (Rc), focal length (f) and the relative error on Rc (and on f). The measured values are D and H; the other data are calculated.

Considering 5% an acceptable value for the relative error, all the results lie on the confidence interval.

To be applied in a control system, this technique requires an appropriate calibration, especially in the measurement of the distance D that directly affects the calculation of f. In fact, our calculation demonstrates that a measurement uncertainty on the distance D is reproduced in a percentage of the same amount on the calculation of f.

[2] The explanation refers to the vertical axis, but it can also be applied to the direction perpendicular to the plane of Fig. 3. This depends on the characteristics of the camera utilized.

Fig. 4. Photo of a ruler taken through the concave mirror.

Table 1
Measurements on a sample mirror.

	RP-mirror dist. D = 600 mm	RP-mirror dist. D = 650 mm	RP-mirror dist. D = 700 mm
H on the ruler (mm)	48	48	48
K_p (-)	1.234	1.258	1.293
S_i (mm)	967	1102	1279
Rc (mm)	3164	3170	3092
f (mm)	1582	1585	1546
Relative error (%)	3.32%	4.01%	1.44%

Table 2
Main characteristics of the images obtained with known profile surfaces.

Type of Surface	Type of Image
Spherical with Rc > 0	Enlarged (magnification)
Spherical with Rc < 0	Reduced (reduction)
Tilted Flat	Shifted (translation)
Cylindrical in *x* (or *y*)	Enlarged only in x (or y) (magnification)
Conical	Translation + magnification differentiated with the radius (distance from the centre)

4. Irregular surfaces

Surfaces with non-spherical, but well identified profiles show predictable image deformations. Table 2 shows the principal characteristics of the images obtained with surfaces with a known profile.

The case of the conical surface is very interesting because it is that of not immediate understanding. Figs. 5 and 6 show how the image of a grid of points changes when viewed through a reflector with truncated conical surface. Fig. 5 presents the Reference Pattern, while

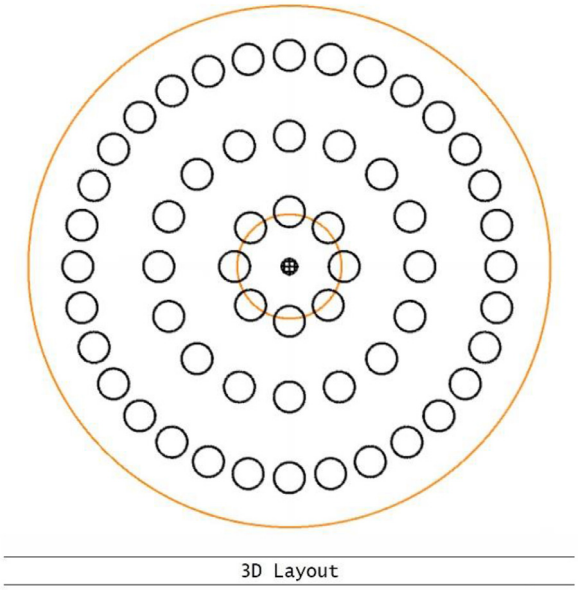

Fig. 5. Reference Pattern and truncated cone mirror.

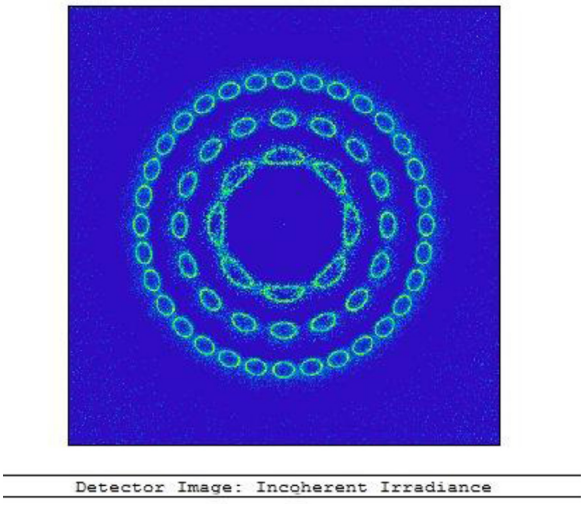

Fig. 6. Simulation results.

Fig. 6 shows the result of the simulation of the measurement, as described in Section 2.

The Reference Pattern in Fig. 5 has been drawn as a series of luminous circles, whose centres are on concentric circumferences with increasing diameter. This circles pattern is reflected by a mirror with truncated conical surface. The two continuous circles, visible in orange in Fig. 5, are the mirror edges.

From the simulations, it is possible to see that the circles change, and the image records a series of shapes, whose axis is placed in a radial direction. Fig. 6 presents the result of a simulation of the luminous circles observed through the truncated conical surface. The circles have increasing magnification towards the centre and the magnification develops only in the direction transverse to the local radius of the cone. The magnification magnitude M depends on the local radius of curvature; in the centre there will be greater magnifications than at the ends. Furthermore, the position of the image is translated towards the outside of the cone with respect to the real object.

Figs. 7 and 8 show how the image of a series of circles changes when viewed through the same reflector with truncated conical surface.

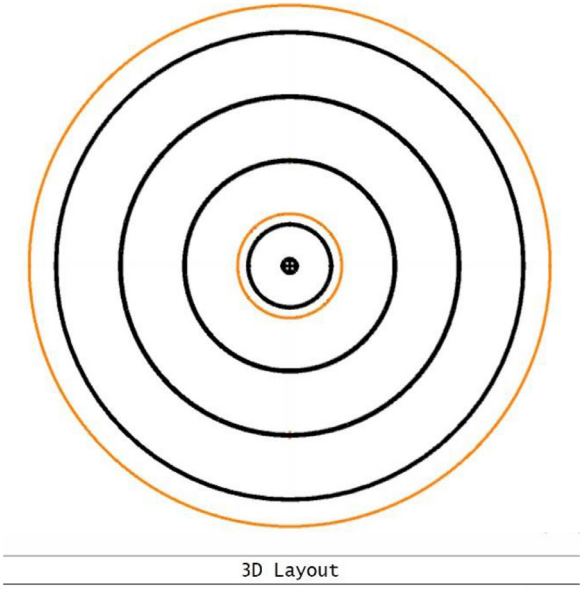

Fig. 7. Reference Pattern and conical mirror.

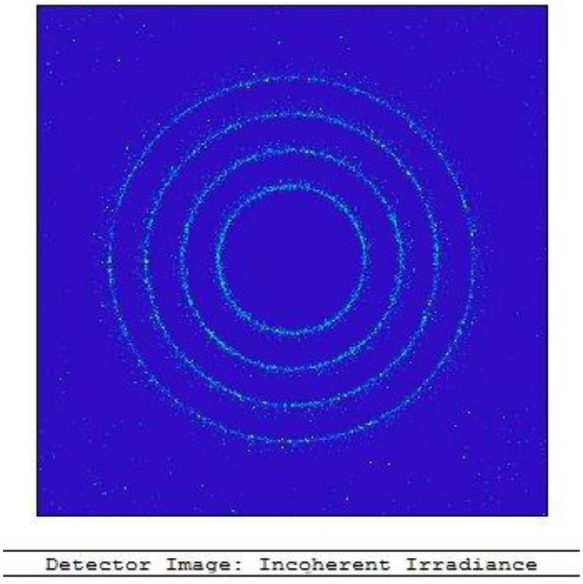

Fig. 8. Simulation results.

Fig. 7 represents a series of circles (in black) placed at a constant distance: the circles in orange are the edges of the mirror. Analogously, the results of the simulation are in Fig. 8. The rings maintain their circular shape, but their radius in Fig. 8 changes with respect to Fig. 7. However, in Fig. 8 the spacing between two successive rings remains constant.

5. Practical example of irregular mirror detection

The method proposed in this article is simple and can be used on mirrors that have long focal length.

When the surfaces have an irregular profile, the radius of curvature changes from point to point so that the image of the Reference Pattern appears distorted in a way that is not easily predictable. The need to study the profile of a particular type of heliostat was an excellent opportunity to test the image study technique. The heliostat under examination (Fig. 9) was obtained from a hexagonal plane mirror by gluing

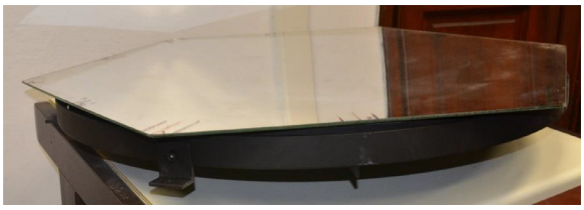

Fig. 9. A photo of the heliostat under examination.

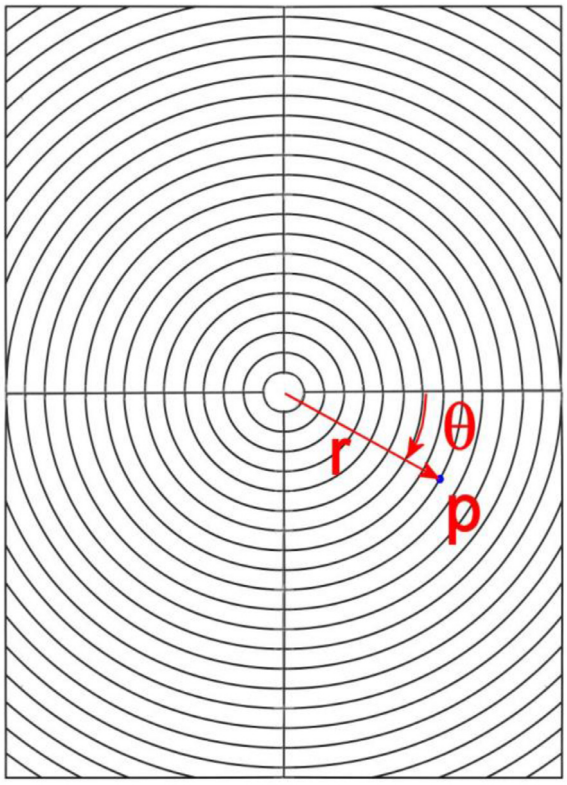

Fig. 10. Test 1: Reference Pattern.

a metal disc to the central rear part of the mirror. A screw connected to the metal disc exerts a traction with the effect of bending the mirror and making it concave. The profile of the mirror, thus deformed, allows the sun's rays to converge but its surface will be very different from the spherical or parabolic one, as can be verified by the images obtained by using the proposed technique with a regular pattern.

The Reference Pattern to be used for this examination is not unique; a wide range of patterns can be used: lattices, circles and lines within which deflections and enlargements can be measured, useful for highlighting the characteristic of interest (rectangular asymmetries, radial asymmetries, linear deformations and in general structural defects). The limits concern their size and the problems related to their positioning and their portability.

Two tests have been conducted on the heliostat, both derived from the simulations illustrated in Section 4. The first one (Test 1) consists in using as Reference Pattern a series of concentric circles, whose radius increases at regular steps. The second one (Test 2) employs as Reference Pattern a set of black dots placed regularly along the concentric circles with increasing radius.

5.1. Test 1 series of circles

The Reference Pattern used in Test 1 is presented in Fig. 10: a lattice formed by concentric circles with increasing radius. The first circle has

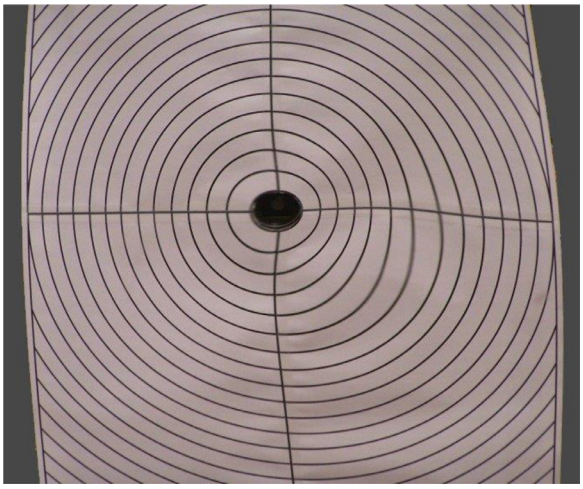

Fig. 11. Test 1: recorded Image, with deformed circles.

a radius of 20 mm, and the radii of the following circles are increased by 20 mm. In Fig. 10 the coordinate system used to locate a point p on the circle is drawn in red. The corresponding image recorded by the camera is reported in Fig. 11.

The point is identified by the coordinates θ and r, so it can be written as: p(θ;r). The angle θ is considered clockwise with respect to the horizontal line, which goes from the centre to the right side, and can vary almost continuously between 0° and 360° The radius r of the circle starts from the centre of the image and has discrete values from 20 to 280 mm in steps of 20 mm.

Even if the mirror under examination was not spherical, it was possible to apply the previous formulas to the deformed image. To do this, two points belonging to two successive circles were considered keeping constant θ. In this way the analysed surface is small and can be approximated with a spherical surface. On this spherical surface the local value of Rc is calculated and therefore the value of f. The surface is sampled by varying the point p along the radii. The graph in Fig. 12 shows the focal length values for four values of θ (0 °, 90 °, 180 ° and 270 °) while r is reported along the horizontal axis. The value of f is attributed to the abscissa value, which corresponds to the average value between the two successive radii considered, therefore the values of the horizontal axis range from 30 to 270 mm.

The graph also reports two averages: the blue dashed line shows the total mean value, while the blue solid line shows the value averaged on the θ values keeping r fixed. This corresponds to making the average following a circumference in the image.

It is possible to notice that there are some values of the radius r where the distribution of the dots has higher dispersion, e.g. r(mm) = 170, 210, 250, 270. This allows to individuate defective zones of the examined heliostat. This analysis presents a problem: keeping constant θ it is not certain that two successive points taken in the deformed image actually correspond to two successive points on the Reference Pattern. With this type of pattern, only radial deformations are detectable.

5.2. Test 2 structure with black dots

For this test, the Reference Pattern was a series of fully filled black circles that are located regularly along the concentric circles with increasing radius. The pattern is observed through the heliostat: this means that the pattern of black dots is reflected by the surface of the mirror under examination. The reflected pattern is deformed, and these local deformations can provide information about surface quality and local slope.

Fig. 13 presents the image of a set of black dots: each dot is characterized by the position of its centre p and has a diameter of 25 mm.

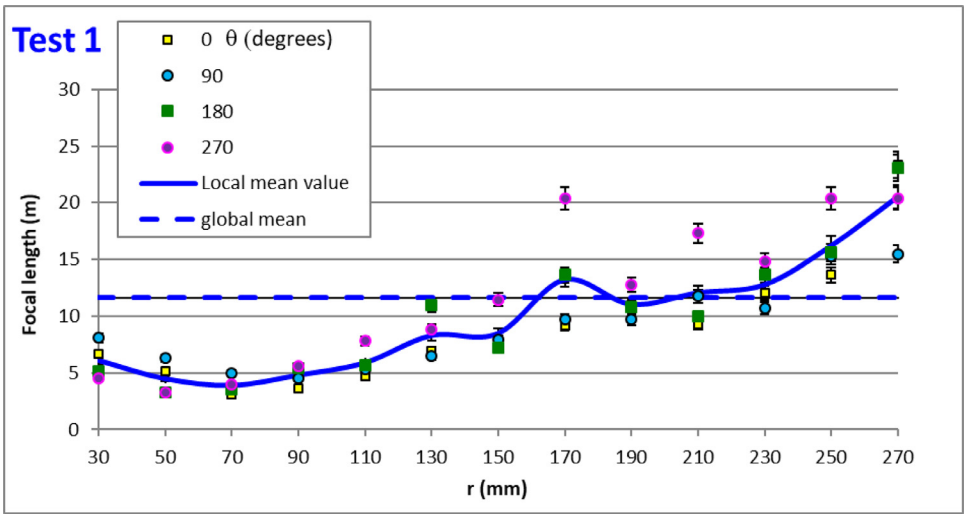

Fig. 12. Test 1: calculated focal length vs circle radius.

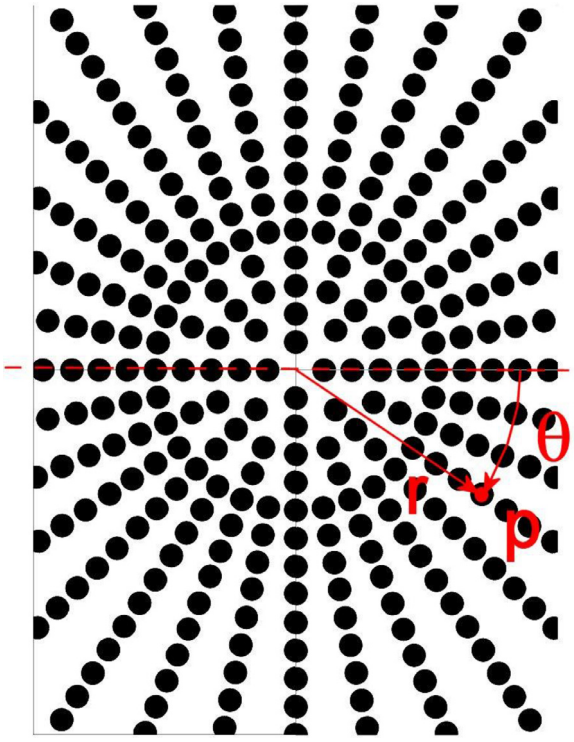

Fig. 13. Test 2: Reference Pattern.

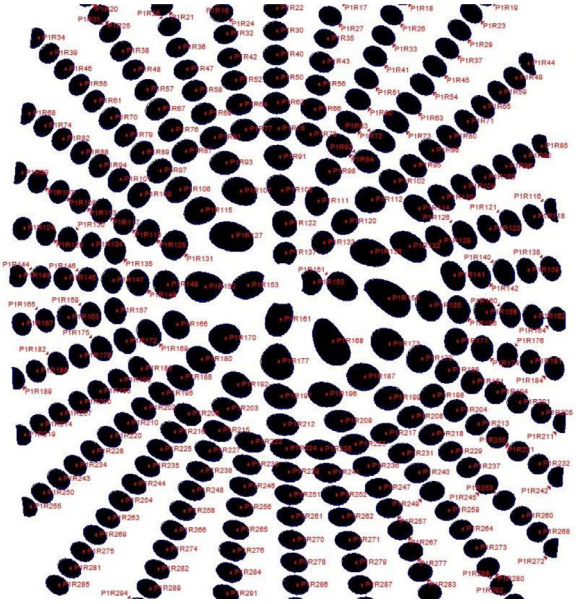

Fig. 14. Test 2: pattern observer through the heliostat, it appears as a deformed image.

As indicated in Fig. 13, the position p is expressed by the distance from the image centre (r) and the angular position in the image (θ), referring to the horizontal line, drawn in red in Fig. 13. The dots are arranged in concentric rings; the distance between two successive rings is 30 mm, so r varies between 30 and 270 mm in steps of 30 mm.

Fig. 14 shows the deformed image analysed by the image processing software. First of all, each dot is identified by an identification number. Then the geometric parameters of the objects identified in the image are calculated. These parameters can be the inclination of the main axis with respect to the vertical or the position of the centroid of the deformed dot.

The dots appear deformed according to different directions, but the majority of the dots beyond the 4th circle ($r > 120$ mm) have taken the shape of an ellipse, whose main axis has an inclination with respect to the horizontal line. This inclination of the axis of the ellipse varies radially as it happens in the simulations in Section 4, which showed how a specular surface with a deformed conical profile deforms the image of a circle in an ellipse.

The graph in Fig. 15 shows the angles of inclination of the main axis of each dot, with respect to the horizontal line. This inclination of the axis of the ellipse is plotted versus the angular position θ of the dot on the concentric circle. The different results, plotted in various colours and with different markers, concern the increasing r-values of the radial coordinate of the dot. The solid black line indicates the ideal inclination that the ellipse axis should have when the dots are reflected by a perfectly conical mirror.

As can be seen from Fig. 13, as the distance r from the centre of the image increases, the number of dots increases. For $r = 30$ mm there are 4 dots, for $r = 60$ mm they are 8, for $r = (90–120)$ mm they are 16 and for the subsequent values of r they become 32.

From the graph in Fig. 15, it can be seen that the surfaces corresponding to the dots with $r > 120$ mm have a trend similar to that of the black ideal line. Therefore, the outermost portion of the figure is similar to a cone.

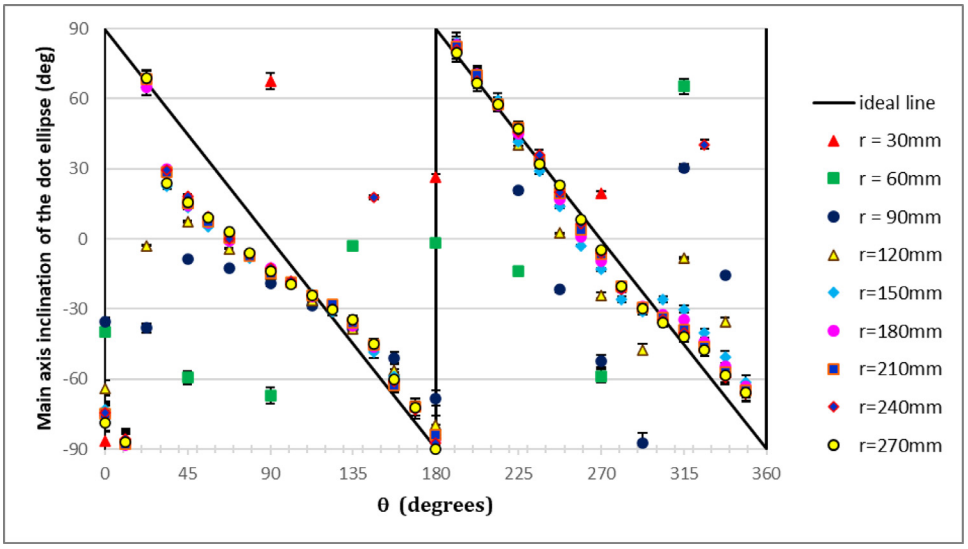

Fig. 15. Test 2: inclination of dot ellipse axis vs dot angular position.

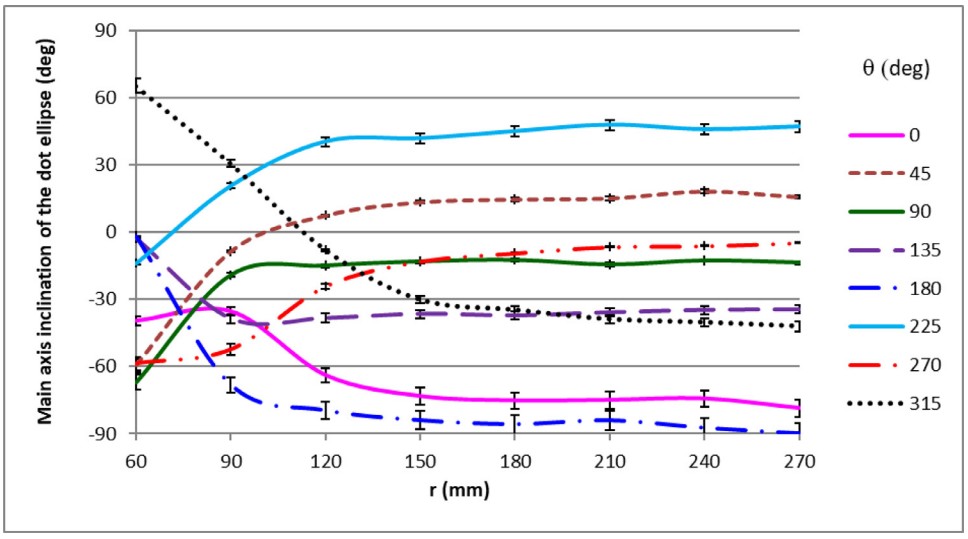

Fig. 16. Test 2: inclination of dot ellipse axis vs dot radius.

The innermost dots appear instead of very variable size and shape, indicating the presence of a more complex surface. It can be seen that the positions of the points relative to $r = 240$ mm show some deformed areas, despite the general trend being the expected one.

As proof of what has been said before, a second analysis was made, which is represented in the graph of Fig. 16. In this case, the dots were analysed in radial lines starting from the centre. The coordinates of the dot centre are r (on the abscissa axis) and θ, which is the parameter that distinguishes the various plotted curves. The ordinate axis reports the inclination of the main axis of the deformed dot (with respect to the horizontal line).

The values of r range from 60 to 270 mm (for $r = 30$ mm there are no points for 45 °, 135 °, 225 ° and 315 °) and 0 ° represents the centre of the pattern. In this analysis, if the mirror profile is conical, the values measured along r would be horizontal lines in Fig. 16, with constant inclination.

The examination of Fig. 16 indicates that the outermost zone has a substantially conical profile, while the central area (with $r < 120$ mm) deviates from it, showing a different trend. This confirms the previous analysis inferred from Fig. 15.

As for Test 1 (using a pattern with a series of circles), the local focal length was obtained using the distance of the centroids of two adjacent dots. Considering the small area, the profile was approximated to a concave mirror and the local focal length was calculated: applying Eq. (3) the curvature radius can be calculated, then the focal length is obtained.

Referring to Test 2 (using a black dots pattern), the dots on the Reference Image were identified by varying r and keeping θ fixed. The results are shown in Fig. 17, reporting the focal length values. The average of the r-values between which the calculation was carried out is associated as abscissa. The various results (plotted as discrete points) correspond to increasing values of θ ; while the solid lines refer to the local and global mean value of the data of the discrete points, as in Fig. 12.

In this case, the points analysed are truly homologous, as the same dots are precisely identified. Information about surface defects can be evinced examining the distribution of each set of points corresponding to each r-value. For example, the distribution of points for $r = 225$ mm is very wide: the f-values range from 12.3 to 28.7 m. This wide spread of the f-values indicates that this is a defective zone for the heliostat, and the most defective point is located at $\Theta = 135$ °.

Similarly, Fig. 17 indicates that the central areas, with $r < 135$ mm, are much less defective; while the lateral zones with $r > 135$ mm are the worst ones.

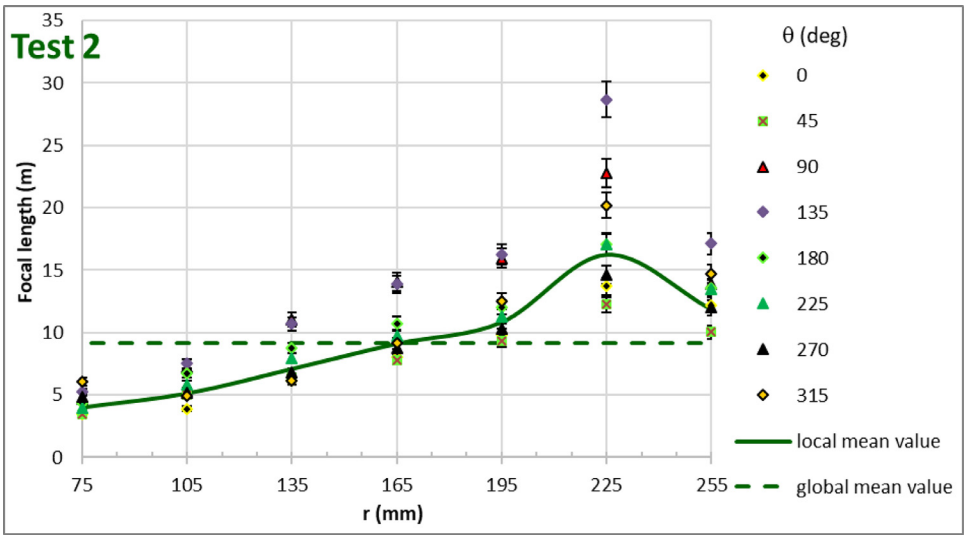

Fig. 17. Test 2: focal length vs dot radius.

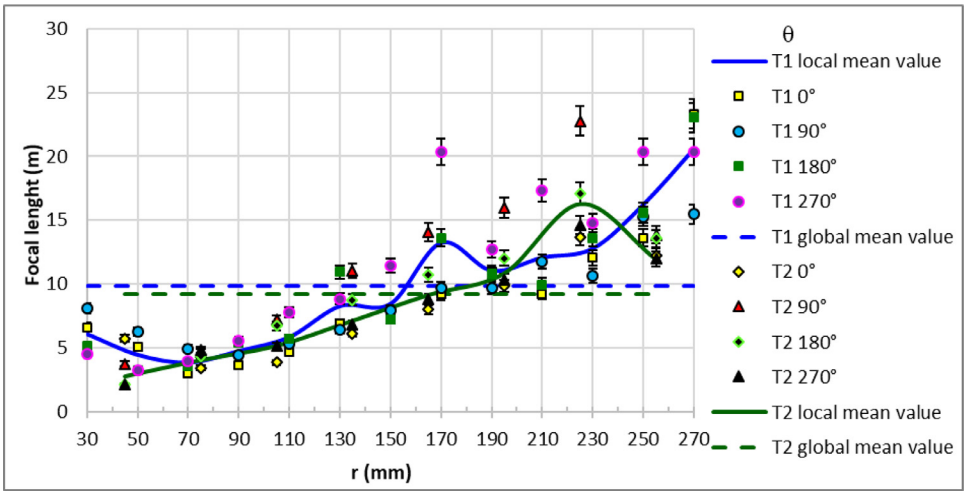

Fig. 18. Comparison of Tests 1 and 2: focal length vs radius.

5.3. Comparison

The comparison between the two tests is also interesting. In both tests, an image of a Reference Pattern is created, which is observed through the same heliostat mirror, and then the deformed image reflected by the mirror is analysed. In Test 1, the Reference Pattern is a grid formed by concentric circles with radius increasing at regular steps. In Test 2, the Reference Pattern is a series of black dots, whose centres are in concentric circles with increasing radius.

Fig. 18 shows the graph of the focal distance for Tests 1 and 2, reporting few data to facilitate the comparison. Only results for angles θ with the values 0 °, 90 °, 180 °, 270 ° are shown.

The round and square markers refer to the measurements made with Test 1 (in steps of 20 mm). The rhomboid and triangular markers report the measurements made with Test 2 (in steps of 30 mm). The blue lines represent the local mean (solid line) and the total mean (dashed line) for Test 1; and similarly, the green lines shown the local and global averages for Test 2 results.

It is interesting to note that the two tests lead to similar average values (for Test 1 f = 9.8 m, for Test 2 f = 9,2 m), also by analysing different areas, at different steps and with different values of radius calculated. It should also be remembered that while for Test 1 the value of θ is indicative of the angle considered on the deformed image acquired, for Test 2 it is indicative of the position of the dot on the Reference Pattern.

From the analysis of the combined results, it can be observed that if you are only interested in controlling the focal length, the simple pattern of Test 1 is sufficient. If, on the other hand, you want to obtain other results such as the correspondence of the mirror shape to the project data, the use of non-continuous patterns as done for Test 2 allows obtaining this information.

6. Conclusions

Controlling the curvature on solar mirrors is essential as the performance of solar collection systems depends on the perfection of the curvature of their solar mirrors. This is particularly crucial when the solar mirrors have large dimensions, like heliostats.

In developing solar collection plants, there is a design phase and an implementation phase. Solar thermal plants are composed of a series of curved reflectors, the heliostats, which focus the sunlight on a receiver typically placed on the top of a tower. The light distribution on the receiver is very sensitive to the curvature of the heliostats. A change in the radius of curvature (or focal length) can worsen the quality of the image focused on the receiver. The curvature (as Rc or f) of every solar mirror is defined in the design phase optimising total collected power and homogeneity of irradiance distribution on the receiver.

Subsequently the heliostats are practically manufactured, and these solar mirrors can contain construction imperfections like local surface defects or, more often, surface deformations of the curvature and asym-

metries. When the manufactured heliostats are mounted in the actual solar field, these surface defects cause an incorrect irradiance distribution on the receiver. Typically, surface imperfections cause a spot enlargement on the receiver. However, the most important effects are the energy losses, which strongly depend on the optical design and concentration characteristics of the heliostat field.

Identifying the causes of these energy losses is the aim of the proposed optical control for solar mirrors. Therefore, for each heliostat it is necessary to know at least the curvature or the focal length. In particular, each solar field contains thousands of heliostats, so it is important to use a quick and economical method of control. The proposed technique is based on the analysis of an image (of a suitable Reference Pattern) reflected by the mirror under test. Exploiting techniques of image analysis, it assesses the mirror surface quality comparing an acquired image with a reference image. The application requires only a photographic camera and a screen with a calibrated pattern.

The technique is simulated and then applied on a real sample of heliostat. Two types of Reference Pattern are considered in the simulations and, correspondingly, two tests are carried out on the same heliostat, using the two Reference Patterns.

The focal distance results for the two tests are compared, and there is a good agreement even if they can evidence different characteristics of the heliostat under examination. Test 1 is able to determine the change in focal length for different zones of the heliostat, whereas Test 2 could also provide some information on the shape of the mirror. The use of non-continuous patterns, as in Test 2, permits to assess the correspondence of the mirror shape to the optical design.

Another important aspect is the possibility of examining different zones of the heliostat. Depending on the industrial manufacturing procedure, each type of heliostat has zones where the defects appear most often.

Using suitable patters, it is possible to apply this method to mirrors of a different shape than mirrors with spherical curvature. As an example, a concave mirror with a truncated cone shape is chosen. Two different patterns are simulated, and the results are comparable.

The design of the pattern is an important step because the difference between what is recorded and what is expected provides the information necessary to confirm the correctness of the realisation of the mirror surface.

The main advantages of the proposed optical control are the low-cost equipment, the ease of application and the simplicity of processing. The results are immediate: the defective areas are immediately visible in the photographic image reflected by the mirror. This optical technique can be customised to examine reflecting surfaces with different shapes and dimensions. Suitable Reference Pattern can be chosen to identify specific deformations, asymmetries, or other particular surface defects of the examined mirror. On an industrial level, this control can be applied during the manufacture of mirrors or on produced samples. Moreover, for industrial control the reference image can be acquired once for all and the camera can be positioned at fixed (known) distance from the samples to be tested. Exemplificative application cases demonstrated the efficacy of the method.

The practical application of this mirror control technique is more difficult on an already existing solar plant than indoor. The principal limitations of the method, when applied to the heliostat in the field, are the dimensions of the screen (depending on the heliostat sizes), the screen positioning, the external light and in general the greater ambient noise. In the laboratory, optical noise can be minimised, and environmental conditions can be monitored, so the laboratory measurement is more accurate and reproducible than in the field.

Authorship contributions

Category 1 Conception and design of study: F. Francini, D. Fontani; acquisition of data: D. Fontani, P. Sansoni; analysis and/or interpretation of data: F. Francini, D. Jafrancesco. Category 2 Drafting the manuscript: D. Fontani, F. Francini, P. Sansoni, D. Jafrancesco; revising the manuscript critically for important intellectual content: D. Fontani, F. Francini, P. Sansoni, D. Jafrancesco. Category 3 Approval of the version of the manuscript to be published (the names of all authors must be listed): D. Fontani, F. Francini, P. Sansoni, D. Jafrancesco.

Declaration of Competing Interest

The authors declare that they have no known competing financial interests or personal relationships that could have appeared to influence the work reported in this paper.

Acknowledgements

All persons who have made substantial contributions to the work reported in the manuscript (e.g., technical help, writing and editing assistance, general support), but who do not meet the criteria for authorship, are named in the Acknowledgements and have given us their written permission to be named. If we have not included an Acknowledgements, then that indicates that we have not received substantial contributions from non-authors.

Supplementary materials

Supplementary material associated with this article can be found, in the online version, at doi:10.1016/j.optlaseng.2021.106835.

References

[1] Briers JD. Optical testing: a review and tutorial for optical engineers. Opt Laser Eng 1999;32:111–38. doi:10.1016/S0143-8166(99)00062-7.
[2] Pottler K, Lupfert E, Johnston GHG, Shortis MR. Photogrammetry: a powerful tool for geometric analysis of solar concentrators and their components. J Sol Energy Eng 2005;127:94–101. doi:10.1115/1.1824109.
[3] Shortis MR, Johnston GHG. Photogrammetry: an available surface characterization tool for solar concentrators, part l: measurements of surfaces. Trans ASME 1996;118:146–50. doi:10.1115/1.2870886.
[4] Stynes JK, Ihas B. Absorber alignment measurement tool for solar parabolic trough collectors. In: Proceedings of the ASME 6th international conference on energy sustainability collocated with the ASME 10th international conference on fuel cell science, engineering and technology; 2012. p. 437–47. ES2012-9128311. doi:10.1115/ES2012-91283.
[5] Stynes JK, Ihas B. Slope error measurement tool for solar parabolic trough collectors. In: Proceedings of the world renewable energy forum, May 13–17; 2012. p. 8.
[6] King P, Sansom C, Comley P. Photogrammetry for concentrating solar collector form measurement, validated using a coordinate measuring machine. Sustainability 2020;12(1):196 20 pages. doi:10.3390/su12010196.
[7] Maccari A, Montecchi M. An optical profilometre for the characterisation of parabolic trough solar concentrators. Sol Energy 2007;81:185–94. doi:10.1016/j.solener.2006.04.004.
[8] Wendelin T, May K, 2007 Gee R. Video scanning hartmann optical testing of state-of-the-art parabolic trough concentrators. In: Proceedings of the international solar energy conference; 2006. ISEC2006-99172:699-707.
[9] Wood RL. Distant-observer techniques for verification of solar-concentrator optical geometry, CA (USA): Lawrence Livermore National Lab; 1981. Technical Report UCRL-53220, ON: DE82021537. https://www.osti.gov/biblio/5119628-distant-observer-techniques-verification-solar-concentrator-optical-geometry (accessed 29 December 2020).
[10] Ulmer S, Heinz B, Pottler K, Lüpfert E. Slope error measurements of parabolictroughs using the reflected image of the absorber tube. J Sol Energy Eng 2009;131:1–5. doi:10.1115/1.3035811.
[11] Francini F, Fontani D, Sansoni P, Mercatelli L, Jafrancesco D, Sani E. Evaluation of surface slope irregularity in linear parabolic solar collectors. Int J Photoenergy 2012;2012:921780 6 pages. doi:10.1155/2012/921780.
[12] QFly-Airborne qualification of CSP plants. An automatic system for inspection and quality assessment of large solar fields, CSP services, concentrating solar power services. http://www.cspfocus.cn/ueditor/net/upload/2019-08-26/bee53691-e6dc-46c5-a47e-dee147fa1af5.pdf (accessed 30 December 2020).
[13] Geng J. Structured-light 3D surface imaging: a tutorial. Adv Opt Photonics 2011;3:128–60. doi:10.1364/AOP.3.000128.
[14] Van der Jeught S, Dirckx JJJ. Real time structured light profilometry: a review. Opt Laser Eng 2016;87:18–31. doi:10.1016/j.optlaseng.2016.01.011.
[15] Marotta G, Sansoni P, Francini F, Jafrancesco D, De Lucia M, Fontani D. Structured light Profilometry on m-PTC. Energies 2020;13:5671 17 pages. doi:10.3390/en13215671.

[16] Huang Lei, Ldir Mourad, Zuo Chao, Asundi Anand. Review of phase measuring deflectometry. Opt Lasers Eng 2018;107:247–57. doi:10.1016/j.optlaseng.2018.03.026.
[17] Guo Chunfeng, Hu Anduo. Three-dimensional shape measurement of aspheric mirrors with null phase measuring deflectometry. Opt Eng 2019;58(10):104102 6 pages. doi:10.1117/1.OE.58.10.104102.
[18] Han Hao, Wu Shiqian, Song Zhan. An accurate calibration means for the phase measuring deflectometry system. Sensors 2019;19:5377 13 pages. doi:10.3390/s19245377.
[19] Burke J, Li W, Heimsath A, von Kopylow C, Bergmann RB. Qualifying parabolic mirrors with deflectometry. J Eur Opt Soc Rapid Publ 2013;8:13014 6 pages. doi:10.2971/jeos.2013.13014.
[20] Faber C, Olesch E, Krobot R, Häusler G. Deflectometry challenges interferometry: the competition gets tougher!. In: Proceedings of the SPIE, 8493; 2012. p. 84930. R15 pages. doi:10.1117/12.957465.
[21] Li W, Sandner M, Gesierich A, Burke J. Absolute optical surface measurementwith deflectometry. In: Proceedings of the SPIE, 8494; 2012. p. 84940. G7 pages. doi:10.1117/12.928690.
[22] Fontani D, Francini F, Mercatelli L, Jafrancesco D, Sansoni P. Colour coded methodology for deformable mirrors. August 2006 issue of. Opt Eng 2006;45(8):080508 3 pages. doi:10.1117/1.2333452.